Controlling interactions in supported bilayers from weak electrostatic repulsion to high osmotic pressure

Arnaud Hemmerle[a,b], Linda Malaquin[a,b], Thierry Charitat[a,1], Sigolène Lecuyer[a,2], Giovanna Fragneto[c], and Jean Daillant[b,d]

[a]Université de Strasbourg, Institut Charles Sadron, Unité Propre de Recherche 22, Centre National de la Recherche Scientifique (CNRS), 67034 Strasbourg Cedex 2, France; [b]Laboratoire Interdisciplinaire sur l'Organisation Nanométrique et Supramoléculaire (LIONS), Service Interdisciplinaire sur les Systémes Moléculaires et les Matériaux (SIS2M), Institut Rayonnement Matière de Saclay (IRAMIS), Commissariat à l'Energie Atomique (CEA), Unité Mixte de Recherche 3299 CEA/CNRS, F-91191 Gif-sur-Yvette Cedex, France; [c]Institut Laue-Langevin, 38042 Grenoble Cedex, France; and [d]Synchrotron SOLEIL, L'Orme des Merisiers, Saint-Aubin, F-91192 Gif-sur-Yvette Cedex, France

Edited by T. C. Lubensky, University of Pennsylvania, Philadelphia, PA, and approved October 19, 2012 (received for review July 9, 2012)

Understanding interactions between membranes requires measurements on well-controlled systems close to natural conditions, in which fluctuations play an important role. We have determined, by grazing incidence X-ray scattering, the interaction potential between two lipid bilayers, one adsorbed on a solid surface and the other floating close by. We find that interactions in this highly hydrated model system are two orders of magnitude softer than in previously reported work on multilayer stacks. This is attributed to the weak electrostatic repulsion due to the small fraction of ionized lipids in supported bilayers with a lower number of defects. Our data are consistent with the Poisson–Boltzmann theory, in the regime where repulsion is dominated by the entropy of counter ions. We also have unique access to very weak entropic repulsion potentials, which allowed us to discriminate between the various models proposed in the literature. We further demonstrate that the interaction potential between supported bilayers can be tuned at will by applying osmotic pressure, providing a way to manipulate these model membranes, thus considerably enlarging the range of biological or physical problems that can be addressed.

interbilayer forces | statistical physics | electrostatic interaction

Supported lipid bilayers offer a unique configuration whereby a single bilayer, accessible to other molecules such as, for example, proteins, peptides, or DNA, is supported on a solid substrate. Beyond their interest for biosensor technology, the access they give to a flat immobilized membrane makes them highly relevant for fundamental studies in biophysics and membrane biology (1, 2). In particular, they provide a unique way to finely characterize the interactions between membranes and their environment, which are not only crucial for membrane fusion and trafficking, endocytosis, and exocytosis (3, 4) but also fascinating from the physical point of view.

Membranes indeed exhibit extremely complex interactions with their environment, in which both molecular-scale enthalpic and fluctuation-related entropic contributions are inextricably involved. In particular, the effect of confinement has been now discussed for 40 years without a definitive answer being found. Helfrich first realized that, in addition to the "direct" electrostatic, van der Waals, and hydration forces (4), the long-range "effective" steric interaction generated by the thermal fluctuations of confined flexible membranes is an essential contribution to the total free energy of interaction (5). Pure hard wall interaction (hard confinement) was first considered in refs. 5 and 6 but is not a realistic description of real systems, and especially not of living ones. Confinement by a "soft" potential was treated either by using self-consistent methods leading to effective exponentially decaying potentials (7–9) or by estimating average values within a full statistical mechanics approach (10). Which functional form should be used to describe entropic repulsion in real experimental situations, however, remains an open question.

Although the surface force apparatus can be used to precisely determine the direct part of the potential (hydration and van der Waals contributions) (11), the entropic repulsion can only be studied by using scattering techniques. Combination with osmotic pressure measurements allowed in particular the determination of the compressibility $B = \partial^2 \mathcal{F} / \partial d_w^2$, where $\mathcal{F}$ is the system free energy and d_w the interlayer water thickness (11, 12). Although some agreement was found with the soft potential of ref. 9, the experimental decay lengths found in ref. 13 were greater than twice the value predicted by theory, ~ 0.2 nm. Moreover, inconsistencies between the temperature dependence of B and the observation of an unbinding transition pointed to the role of static defects in multilayers, which would dramatically affect bilayer interactions (14). In the work described here, we determine the interaction potential between supported bilayers. These bilayers can be almost defectless but contain much less material than multilayers and could not be studied using diffuse scattering until recently (15).

Results and Discussion

Two kinds of supported bilayers were investigated in this study, both consisting of two bilayers (Fig. 1). The first type, called "double bilayers" in the following, consists of two bilayers of $L-\alpha$ 1,2-distearoyl-sn-glycero-3-phosphocholine (DSPC), whereas in the other, called "OTS-bilayer," the first monolayer close to the substrate is replaced by an octadecyl-trichlorosilane (OTS) grafted layer (details in *Materials and Methods*). In both cases, the second bilayer is free to fluctuate in the potential of the first bilayer and of the substrate. A combined fit of specular and off-specular data is performed to increase sensitivity, using a model taking into account the static and thermal roughness from both bilayers (ref. 16 and *Materials and Methods*). From the fits presented in Fig. 2, we obtain structural parameters, in particular the bilayer–bilayer distance and the interlayer water thickness, but also the interaction potential second derivative and the bilayer tensions and bending rigidities (Fig. 3). Electron density profiles for OTS or double bilayers can be found in ref. 16. (An example is given in *SI Materials and Methods*.)

In all cases, the best-fit value for the floating membrane tension is 0.3 ± 0.2 mN/m. The bending rigidity decreases from $(250 \pm 50) k_B T$ in the gel phase (T = 42.9 °C) to $(50 \pm 20) k_B T$ in the fluid phase (T = 52.9 °C), in agreement with previously

Author contributions: T.C., G.F., and J.D. designed research; A.H., L.M., T.C., S.L., G.F., and J.D. performed research; A.H., L.M., T.C., S.L., and J.D. analyzed data; and A.H., T.C., and J.D. wrote the paper.

The authors declare no conflict of interest.

This article is a PNAS Direct Submission.

[1]To whom correspondence should be addressed. E-mail: thierry.charitat@ics-cnrs.unistra.fr.

[2]Present address: Laboratoire Interdisciplinaire de Physique, Unité Mixte de Recherche, Université Joseph Fourier, and Centre National de la Recherche Scientifique, 38402 Saint Martin d'Heres, France.

This article contains supporting information online at www.pnas.org/lookup/suppl/doi:10.1073/pnas.1211669109/-/DCSupplemental.

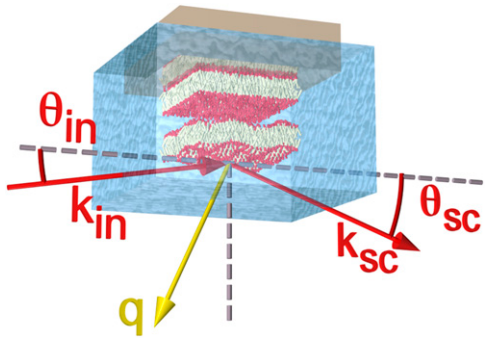

Fig. 1. Schematic view of the experimental setup for specular and off-specular reflectivity. The grazing and scattered wavevectors (respectively angles of incidence) are $\mathbf{k}_{in}$ and $\mathbf{k}_{sc}$ (respectively θ_{in} and θ_{sc}). $\mathbf{q}$ is the wavevector transfer.

reported values (15). The static, substrate-induced roughness of both membranes is always less than 0.3 nm and remains constant, as well as the thermal roughness $\sigma_{th,1}$ of the first, adsorbed membrane, which is on the order of 0.4–0.5 nm (Fig. 4, *Inset*). The thermal roughness $\sigma_{th,2}$ of the second bilayer is larger than that of the first bilayer, justifying the denomination "floating bilayer," in good agreement with previous experiments (16, 17).

A zoom of the off-specular reflectivity in the region where it is most sensitive to the interaction potential is shown in Fig. 2 for different temperatures. It is important to note here that the second derivative of the interbilayer interaction potential is directly linked to the depth of the minimum in the diffuse scattering curve around $q_z \approx 1.0 - 1.5$ nm^{-1}, without much coupling

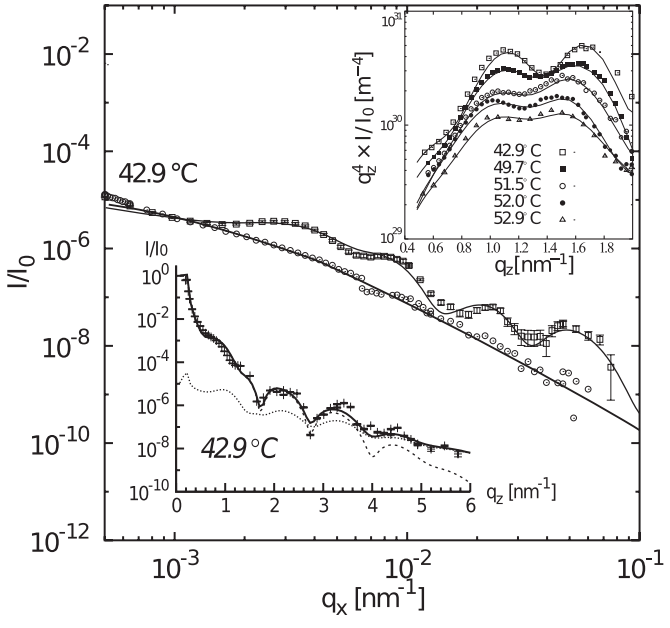

Fig. 2. Off-specular reflectivity from silicon substrate (open circles) and an OTS bilayer at $T = 42.9$ °C (open squares) as a function of q_x. Continuous lines represent best fits. (*Upper Inset*) Off-specular reflectivity as a function of q_z zoomed in the region where it is most sensitive to the potential at $T = 42.9$ °C (open squares), 49.7 °C (filled squares), 51.5 °C (open circles), 52.0 °C (filled circles), and 52.9 °C (open triangles). Note the shift in minimum position and decrease in contrast with increasing temperature. (*Lower Inset*) Specular reflectivity (continuous line), "true" specular reflectivity (dashed line), and diffuse scattering in the specular direction $q_x = 0$ (dotted line) calculated using the model of ref. 16 using the fit parameters and experimental resolution.

to the other parameters. Similarly, the interlayer water thickness is strongly correlated to the q_z position of that minimum. Hence, it can be seen directly in Fig. 2, *Inset*, that the interaction potential becomes weaker (the minimum is less pronounced) when the interlayer water thickness increases (left shift of the minimum) at higher temperatures.

The second derivative of the interbilayer potential U''_{12} obtained by fitting the experimental data is represented as a function of the interlayer water thickness d_w in Fig. 3, where our data are compared with values obtained by Petrache et al. for Egg PC multilayers (13). Remarkably, our samples are more hydrated than multilayers (d_w is 0.1–0.5 nm larger) and interact via a softer interaction potential (U''_{12} is smaller). Note that in this analysis the interaction potential is not only strongly constrained via its second derivative U''_{12} but also via d_w, which fixes the position of its minimum. d_w is in turn reported as a function of the second bilayer thermal roughness $\sigma_{th,2}$ in Fig. 4, which shows a strong correlation between the two parameters, demonstrating that there is a large entropic contribution to the repulsion as expected.

The accuracy of our data, in particular for large separations, allows for a precise assessment of the repulsive part of the potential. In particular, it allows for a test of the different functional forms that have been used in the literature to model the entropic part of the potential. With this aim, we first accurately calculated the attractive part of the potential using the Lifshitz theory (18), carefully modeling the silicon-silicon oxide-water-lipid bilayer-water-lipid bilayer stack (more details in *SI Materials and Methods*). For $d_w < 3$ nm, a good approximation to the van der Waals interaction energy is $U_{\mathrm{vdW}} = -H/12\pi(d_w + 2d_{\mathrm{head}})^2$, with $H = 5.3 \times 10^{-21}$ J and d_{head} the headgroup layer thickness (0.4–0.8 nm), in good agreement with previous work (19, 20).

We further modeled hydration forces using a classic exponential decay, $U_{\mathrm{hyd}} = P_h z_h \exp(-z/z_h)$, with $P_h = 1 - 5 \times 10^7$ Pa the hydration pressure and $z_h = 0.16 - 0.2$ nm the hydration length (13).

The renormalization of the microscopic interaction potential by the thermal fluctuations is a complex problem of modern statistical physics. According to Helfrich (21), the membrane free energy is the sum of the microscopic potential and of the entropy cost of confining the flexible membrane, which results in an effective potential controlling bilayer position. The effective potential, average bilayer position, and fluctuation amplitude are thus coupled quantities that must be self-consistently determined.

As mentioned in the Introduction, Podgornik and Parsegian have extended Helfrich's approach (21) to take into account hydration repulsion and van der Waals attraction in the so-called "soft" potential (9), and the self-consistent approaches of refs. 10 and 22 allow the calculation of average position, rms roughness, and mean effective potential curvature. All these theories are based on a quadratic approximation of the interaction potential, either symmetric (21) or not (9, 10, 22). In any case, a non-symmetric case, like ours, can always be mapped to a symmetric case by identifying the strength of the quadratic potential with the second derivative of the asymmetric potential. As an example, the Helfrich potential has been shown to correctly describe a supported bilayer interacting with a single hard wall in the limit of small fluctuations (see ref. 10 and *SI Materials and Methods*).

We first considered hard wall repulsion, with $U_{\mathrm{Hel}} = c_H/\kappa(k_B T/z)^2$ (21) per unit area and c_H ranging from 0.08 to 0.2 (10, 23). The corresponding d_w equilibrium values at zero applied pressure are given by the dark gray area on Fig. 3 and show poor agreement with the data. As expected, the hard-wall potential also fails to describe the d_w vs. $\sigma_{th,2}$ curves (Fig. 4). Accordingly, the classic "Helfrich Ansatz" $d_w \propto \sigma_{th}$ does not apply (Fig. 4). We also note that simply shifting the zero of the potential to account for softness does not help and that the potential of ref. 6 taking membrane tension into account cannot be distinguished from the hard-wall potential for realistic tension values. The "soft" potential of Podgornik and Parsegian (9) $U_{\mathrm{soft}} =$

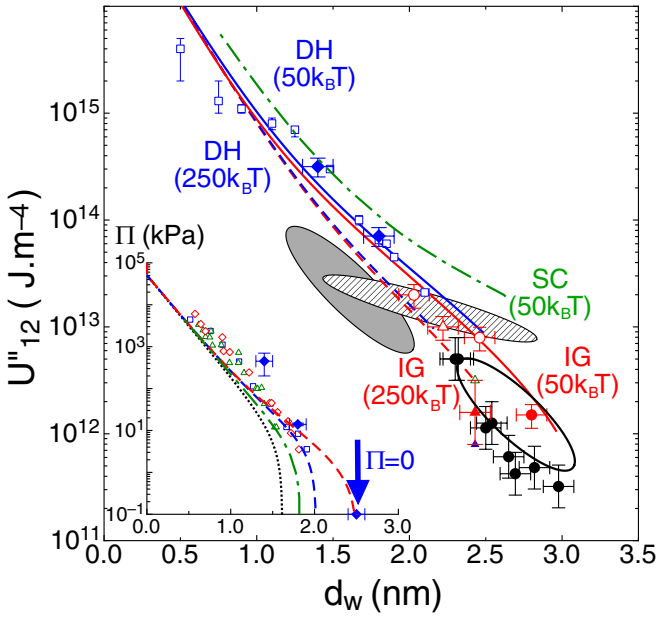

Fig. 3. Interaction potential second derivative U''_{12} as a function of the interlayer water thickness d_w. (open blue squares): data from Petrache et al. (13) for Egg PC in fluid phase. All other data from this work using DSPC: fluid phase (filled black circles); fluid phase before (filled red circles) and after (open red circles) the addition of salt ($T = 58$ °C; $\ell_D = 0.5$ nm and 0.4 nm); gel phase before (filled red triangles) and after (open red triangles) the addition of salt ($T = 40$ °C; $\ell_D = 0.4$ nm); filled blue diamonds: Gel Phase with applied osmotic pressure ($\Pi = 10 \pm 4$ and 450 ± 250 kPa). Red solid (respectively dashed) lines: soft-confinement potential (9) plus electrostatic contribution in the Ideal Gas limit (IG) for Fluid (respectively Gel) phase. Blue solid (respectively dashed) lines: soft-confinement potential (9) plus electrostatic contribution in the Debye-Hückel limit (DH) ($\ell_D = 0.3$ nm) for Fluid (respectively Gel) phase. Green dashed-dotted line: self-consistent model (10) in fluid phase ($\kappa = 50 k_B T$). The ellipses show the region of equilibrium states without applied pressure for Helfrich, hydration, and van der Waals forces (gray area); soft-confinement, hydration, and van der Waals forces (dashed area); soft-confinement, hydration and van der Waals forces plus electrostatic interaction in the ideal gas limit (empty ellipse). The different ellipses were obtained by varying P_h, z_h, d_{head}, and κ within the limits indicated in text. (*Inset*) Osmotic pressure Π (interaction potential first derivative U'_{12}) as a function of the interlayer water thickness d_w. Open symbols: data from Petrache et al. (13) for Egg PC (open blue squares), 1,2-Dimyristoyl-sn-glycero-3-phosphocholine (open red diamonds), and 1,2-dipalmitoyl-*sn*-glycero-3-phosphocholine (open green triangles) in fluid phase. Filled blue diamonds: data from this work using DSPC in gel phase with applied osmotic pressure. Red dashed line: soft-confinement potential (9) with electrostatic contribution in the Ideal Gas limit for the Gel phase. Blue dashed line: soft-confinement potential (9) plus electrostatic contribution in the Debye-Hückel limit (DH) ($\ell_D = 0.3$ nm) for the Gel phase. Green dashed-dotted line: self-consistent model (10) in gel phase ($\kappa = 250 k_B T$). Black dotted line: microscopic potential plus electrostatic contribution without any entropic contribution. The same set of parameters has been used in main figure and in the *Inset*.

$\pi k_B T/16\sqrt{P_h/\kappa/z_h}\exp(-z/nz_h)$ leads to a slightly better agreement but still predicts U''_{12} values one to two orders of magnitude larger than those observed experimentally (Fig. 3) and also underestimates the values of d_w and $\sigma_{th,2}$ data (Fig. 4). Finally, the self-consistent theory of ref. 10, which in principle allows one to calculate the mean d_w, U''_{12}, or $\sigma_{th,2}$ more satisfactorily than effective potential theories, is indeed in good agreement with the d_w vs. $\sigma_{th,2}$ data, but it strongly overestimates d_w, σ_{th}, and U''_{12}, probably because of a bad sampling of the most confined microstates.

Because our bilayers weakly interact with the substrate and can be very close to detachment, which was sometimes observed for temperatures $\gtrsim 60°$ C, a very small but long-range repulsive contribution to the potential would in fact be enough to shift the equilibrium position to higher d_w and lower U''_{12}. Such electrostatic interactions are investigated in ref. 24 but always ignored in scattering studies on zwitterionic lipids (13). Phosphatidylcholines indeed present *pKa* values of 2.7 and 11 (25) and bear a positive charge density $\sigma \sim 0.001$ e/nm^2 at the experimental pH = 5.5. This small amount of charges, necessarily present owing to the amphoteric character of the phosphatidylcholine group, leads to a weak electrostatic repulsion that was recently shown sufficient to prevent vesicles from adhering (26).

In our experiments, surface charge densities are small, and the mean-field Poisson–Boltzmann theory is expected to appropriately describe the system. For DSPC supported bilayers in ultrapure water, the Gouy–Chapman length related to the surface charge density σ is $\ell_G \sim 10^2 - 10^3$ nm, and the Debye–Hückel length that describes screening is $\ell_D \sim 200 - 500$ nm and $d_w \sim 2 - 3$ nm. In this regime, the Ideal Gas limit of the mean-field Poisson–Boltzmann theory, where the interaction potential reads $U_{el} = 2k_B T\sigma/e\ln(d_w)$, should apply rather than the Debye–Hückel limit (27). Adding this contribution to the soft potential of ref. 9 gives a perfect description of our data for both representations U'_{12} vs. d_w (Fig. 3) and d_w vs. $\sigma_{th,2}$ (Fig. 4). Adding the electrostatic contribution extends the curves previously obtained to larger $\sigma_{th,2}$ and d_w without significantly modifying their low d_w part. Therefore, it cannot significantly improve the agreement for the other forms of the potential (Fig. 3). Accordingly, the charge density is very robust and does not depend on the other parameters. The validity of the soft effective potential in the presence of electrostatic interactions could nevertheless be questioned because the soft potential was explicitly constructed for hydration and van der Waals forces only. Although the influence of electrostatic interaction on entropically induced repulsive forces has not been investigated in detail, these are very long range compared with van der Waals and hydration interactions and should be only marginally renormalized. Moreover, it was shown in ref. 27 that in the absence of van der Waals and

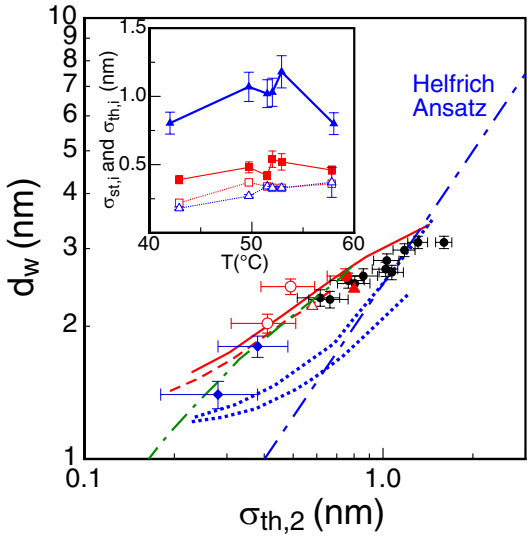

Fig. 4. d_w as a function of $\sigma_{th,2}$. Symbols are the same as for Fig. 3. Dashed-dotted line (blue online): "Helfrich Ansatz" $d_w^2 = 1/6\sigma_{th,2}^2$. Dotted lines (blue online): Helfrich confinement, with a 0.3-nm shift for the lower curve as explained in text. Dashed line (red online): soft potential (9) without electrostatic contribution. Solid line (red online): Soft potential (9) with electrostatic contribution. Green dashed-dotted line: self-consistent model (10) with electrostatic contribution. (*Inset*) Static roughness $\sigma_{st,i}$ (open symbols) and thermal roughness $\sigma_{th,i}$ (closed symbols) of the first strongly adsorbed bilayer (i = 1, square, red online) and of the floating bilayer (i = 2, triangle, blue online).

hydration forces, the renormalization of electrostatic interactions is negligible in the limit where the in-plane electrostatic correlation length ξ (50–100 nm here) is larger than d_w.

To further check the effect of electrostatic interactions, NaCl was added to a double bilayer. This is expected to increase screening and is easier to analyze than changing the pH to change the lipids degree of ionization. We prepared two solutions with $\ell_D = 0.45$ nm and $\ell_D = 0.3$ nm (*Materials and Methods*). The results are reported in Figs. 3 and 4. A strong decrease in the interlayer water thickness d_w and in the thermal roughness $\sigma_{th,2}$ is observed, as well as a large increase in the interbilayer potential U''_{12}, in good agreement with the strong screening of the electrostatic potential.

A further proof of the good control we have over the interactions between supported bilayers is provided in Fig. 3, *Inset*, where the effect of osmotic pressure is shown. Osmotic pressure was applied using polyvinylpyrrolidone (PVP) (details in *Materials and Methods*), and here again, the agreement with the theoretical model and with previous experiments on multilamellar systems is perfect. This is a demonstration that the interbilayer potential of supported bilayers can be tuned using osmotic pressure, allowing us to extend the measurements toward smaller interlayer water thicknesses and to bridge the gap with multilayer studies.

Conclusion

In this article, X-ray off-specular scattering measurements of the interaction potential between two bilayers adsorbed on a solid substrate are shown to lead to results presenting unprecedented sensitivity, illustrated by the necessity of taking into account the very weak electrostatic repulsion between almost neutral bilayers and the possibility of discriminating between different entropic and electrostatic potentials. These results show that supported bilayers are significantly more hydrated and therefore exhibit more intrinsic properties than the usually studied multilayers, possibly owing to defects in the latter. This opens up a wide range of possibilities for understanding unbinding or investigating the effect of various biological molecules on interaction and adhesion between membranes.

Materials and Methods

The supported bilayers were prepared by depositing two bilayers on ultra-flat silicon substrates (SESO), where the first, more strongly adsorbed, bilayer is either a bilayer of DSPC (Avanti Polar Lipids) made by a combination of classical Langmuir-Blodgett (LB) and Langmuir-Schaefer (LS) depositions (vertical sample) (28) or a mixed OTS–lipid bilayer (OTS bilayers), where the OTS layer is chemically grafted on the substrate (29). A second, "floating" bilayer is then prepared by a LB deposition, followed by an LS deposition. The first bilayer serves both as a spacer to reduce the interaction between the floating bilayer and the substrate and keep it free to fluctuate, and to investigate bilayer–bilayer interactions. The sample is then inserted into a polytetrafluoroethylene sample cell with 50-μm-thick windows. The sample cell is tightly closed and transferred to an alumina box, thermalized by a water circulation, first at 25 °C, then heated by steps, with a feedback on the temperature measured inside the sample cell by a PT100 resistance.

Experiments were performed using ultra-pure water (18.2 MΩ.cm), obtained from a Millipore purification system. Dissolution of CO in water leads to Debye-Length values around ∼200 nm, 10 times smaller than the 960 nm expected for such samples (30). By adding sodium chloride $c = 0.5$ and 1 M, we obtained solutions with Debye length equal to 0.45 and 0.3 nm, respectively. Osmotic pressure was applied using PVP of average molecular weight 40,000 (Sigma Aldrich) mixed with milli-Q water. Solutions of 4% and 30% PVP (wt/wt) were prepared and homogenized with magnetic stirrings overnight. The bulk water was then carefully replaced by the PVP/water solutions with syringes, taking care not to expose the bilayers to air. The values of the osmotic pressures are deduced from the PVP concentrations as calculated by Vink (31) and reported in ref. 32, leading to $\Pi = 14 \pm 2$ kPa and 450 ± 250 kPa.

Specular and off-specular reflectivities were recorded using the procedure of ref. 15. The experiments reported here used a 27-keV X-ray beam (wavelength $\lambda = 0.0459$ nm) at the Collaborating Research Group-InterFace beamline of the European Synchrotron Radiation Facility (ESRF). The scattering geometry is described in Fig. 1. The monochromatic incident beam was first extracted from the polychromatic beam using a two-crystal Si(111) monochromator. Higher harmonics were eliminated using a W-coated glass mirror, also used for focusing. In all experiments, the incident beam was 500 μm × 18 μm [horizontal (H) × vertical (V)]. The reflected intensity was defined using a 20 mm × 200 μm (H × V) slit at 210 mm from the sample and a 20 mm × 200 μm (H × V) slit at 815 mm from the sample and recorded using a NaI(Tl) scintillator. Specular reflectivity was obtained by rocking the sample for each angle of incidence (q_x scans for approximately constant q_z) to subtract the background. Off-specular reflectivity was measured at a constant grazing angle of incidence of 0.7 mrad below the critical angle of total external reflection at the Si–water interface (0.83 mrad), leading to variation of both q_x and q_z (Fig. 1).

Optimization of slit widths allowed us to extend the in-plane wavevector transfer range $q_\parallel$ by 1 order of magnitude from 2×10^6 m to 2×10^5 m compared with the experiments of ref. 15. Our experiment is thus sensitive to the off-specular diffusion by both bilayers and not only the more strongly fluctuating one, allowing for a precise determination of interaction potentials.

The differential scattering cross-section (power scattered per unit solid angle per unit incident flux) can be written (16):

$$\frac{d\sigma}{d\Omega} \approx r_e^2 \left|t(\theta_{\text{in}})\right|^2 \left|t(\theta_{\text{sc}})\right|^2 \left\langle \left| \int dr e^{iq_\parallel \cdot r_\parallel} \left[\frac{\rho_{Si} - \rho_w}{iq_z} e^{iq_z z_s(r_\parallel)} + \delta\tilde{\rho}_1(q_z) e^{iq_z z_1(r_\parallel)} + \delta\tilde{\rho}_2(q_z) e^{iq_z z_2(r_\parallel)} \right] \right|^2 \right\rangle, \quad [1]$$

where $r_e = 2.818 \times 10^{-15}$ m, $t(\theta_{\text{in}})$, and $t(\theta_{\text{sc}})$ are the Fresnel transmission coefficients between water and silicon, for the grazing angle of incidence θ_{in} and for the scattering angle θ_{sc}. The coefficient $t(\theta_{\text{in}})$ represents a good approximation to the actual field at the interface, whereas $t(\theta_{\text{sc}})$ describes how the scattered field propagates to the detector. Eq. **1** has to be multiplied by the incident flux and (numerically) integrated over the detector solid angle to get the scattered intensity. The three terms in between the square brackets describe the surface roughness and bilayers 1 and 2 static roughness and thermal fluctuations, respectively. $\delta\tilde{\rho}_i(q_z)$ (i = 1,2) is the Fourier transform of the i-th bilayer [located at $z_i(r_\parallel)$] electron density profiles (form factors), which are described using the so-called 1G-hybrid model (16, 33). Expanding the square modulus in Eq. **1**, we get self- and cross- height–height correlation functions of the substrate and bilayers, where the cross-correlations are sensitive to the interaction potentials.

We describe the substrate correlation function using a self-affine correlation function (34). Static and thermal correlation functions used in Eq. **1** are derived in detail in ref 16 using the free energy:

$$\tilde{\mathcal{F}}_q = \frac{1}{2} \sum_{i=1}^{2} \left[\left(\tilde{a}_i(q_\parallel) + U''_{12} \right) \left| \tilde{z}_i(q_\parallel) \right|^2 + U''_{is} \tilde{z}_i(q_\parallel) \tilde{z}_s(-q_\parallel) \right] - U''_{12} \tilde{z}_1(q_\parallel) \tilde{z}_2(-q_\parallel), \quad [2]$$

with $\tilde{a}(q_\parallel) = U''_{is} + \gamma_i q_\parallel^2 + \kappa_i q_\parallel^4$, where γ_i and κ_i are, respectively, the tension and the bending modulus of the i-th bilayer. U''_{is} and U''_{12} are second derivatives of the effective interaction potential between the substrate and a bilayer and between bilayers. The linear response theory of Swain and Andelman (35) was extended to double bilayers to describe the static coupling of the bilayers to the substrate, and the thermal correlation functions were derived by diagonalizing $\tilde{\mathcal{F}}_q$, applying the equipartition of energy and Fourier transforming.

ACKNOWLEDGMENTS. We thank J.-S. Micha for assistance during the experiments at ESRF (BM32), the Institut Laue-Langevin for support laboratories for sample preparation, and P. Kékicheff and C. Marques for stimulating discussions.

1. Sackmann E (1996) Supported membranes: Scientific and practical applications. *Science* 271(5245):43–48.
2. Castellana ET, Cremer PS (2006) Solid supported lipid bilayers: From biophysical studies to sensor design. *Surf Sci Rep* 61:429–444.
3. Mouritsen O, Andersen O (1998) In search of a new biomembrane model. *Biol Skr Dan Vid Selsk* 49:1–214.
4. Lipowsky R (1995) Generic interactions of flexible membranes. *Structure and Dynamics of Membranes*, eds Lipowsky R, Sackmann E (Elsevier, Amsterdam), Vol 1, pp 521–602.

5. Helfrich W (1973) Elastic properties of lipid bilayers: Theory and possible experiments. *Z Naturforsch C* 28(11):693–703.
6. Seifert U (1995) Self-consistent theory of bound vesicles. *Phys Rev Lett* 74(25): 5060–5063.
7. Evans EA, Parsegian VA (1986) Thermal-mechanical fluctuations enhance repulsion between bimolecular layers. *Proc Natl Acad Sci USA* 83(19):7132–7136.
8. Sornette D, Ostrowsky N (1986) Importance of membrane fluidity on bilayer interactions. *J Chem Phys* 84:4062–4067.
9. Podgornik R, Parsegian V (1992) Thermal-mechanical fluctuations of fluid membranes in confined geometries: the case of soft confinement. *Langmuir* 8:557–562.
10. Mecke KR, Charitat T, Graner F (2003) Fluctuating lipid bilayer in an arbitrary potential: Theory and experimental determination of bending rigidity. *Langmuir* 19: 2080–2087.
11. Rand RP, Parsegian VA (1989) Hydration forces between phospholipid bilayers. *Biochim Biophys Acta* 988:351–376.
12. Nagle JF, Tristram-Nagle S (2000) Structure of lipid bilayers. *Biochim Biophys Acta* 1469(3):159–195.
13. Petrache HI, et al. (1998) Interbilayer interactions from high-resolution x-ray scattering. *Phys Rev E Stat Phys Plasmas Fluids Relat Interdiscip Topics* 57:7014–7024.
14. Vogel M, Münster C, Fenzl W, Salditt T (2000) Thermal unbinding of highly oriented phospholipid membranes. *Phys Rev Lett* 84(2):390–393.
15. Daillant J, et al. (2005) Structure and fluctuations of a single floating lipid bilayer. *Proc Natl Acad Sci USA* 102(33):11639–11644.
16. Malaquin L, Charitat T, Daillant J (2010) Supported bilayers: Combined specular and diffuse X-ray scattering. *Eur Phys J E Soft Matter* 31(3):285–301.
17. DeCaro CM, et al. (2011) Substrate suppression of thermal roughness in stacked supported bilayers. *Phys Rev E Stat Nonlin Soft Matter Phys* 84(4 Pt 1):041914.
18. Shubin VE, Kékicheff P (1993) Electrical double layer structure revisited via a surface force apparatus: Mica interfaces in lithium nitrate solutions. *J Colloid Interface Sci* 155:108–123.
19. Marra J, Israelachvili J (1985) Direct measurements of forces between phosphatidylcholine and phosphatidylethanolamine bilayers in aqueous electrolyte solutions. *Biochemistry* 24(17):4608–4618.
20. Parsegian V (1993) Reconciliation of van der waals force measurements between phosphatidylcholine bilayers in water and between bilayer-coated mica surfaces. *Langmuir* 9:3625–3628.
21. Helfrich W (1978) Steric interaction of fluid membranes in multilayer systems. *Zeitschrift für Naturforschung* 33:305–315.
22. Manghi M, Destainville N (2010) Statistical mechanics and dynamics of two supported stacked lipid bilayers. *Langmuir* 26(6):4057–4068.
23. Gompper G, Kroll DM (1989) Steric interactions in a multimembrane system: A Monte-Carlo study. *Europhys Lett* 9:59.
24. Cowley AC, Fuller NL, Rand RP, Parsegian VA (1978) Measurement of repulsive forces between charged phospholipid bilayers. *Biochemistry* 17(15):3163–3168.
25. Sandén T, Salomonsson L, Brzezinski P, Widengren J (2010) Surface-coupled proton exchange of a membrane-bound proton acceptor. *Proc Natl Acad Sci USA* 107(9): 4129–4134.
26. Pincet F, Cribier S, Perez P (1999) Bilayers of neutral lipids bear a small but significant charge. *Eur Phys J B* 11:127–130.
27. Andelman D (1995) Electrostatic properties of membranes: The poisson-boltzmann theory. *Structure and Dynamics of Membranes*, ed Sackmann E (Elsevier Science, Amsterdam), pp 603–642.
28. Charitat T, Bellet-Amalric E, Fragneto G, Graner F (1999) Adsorbed and free lipid bilayers at the solid-liquid interface. *Eur Phys J B* 8:583–593.
29. Hughes AV, Goldar A, Gestenberg MC, Roser SJ, Bradshaw J (2002) A hybrid sam phospholipid approach to fabricating a free supported lipid bilayer. *Phys Chem Chem Phys* 4:2371–2378.
30. Haughey D, Earnshaw JC (1998) Studies of colloidal interactions using total internal reflection microscopy. *Colloids Surf A Physicochem Eng Asp* 136:217–230.
31. Vink H (1971) Precision measurements of osmotic pressure in concentrated polymer solutions. *Eur Polym J* 7:1411–1419.
32. McIntosh TJ, Simon SA (1986) Hydration force and bilayer deformation: A reevaluation. *Biochemistry* 25(14):4058–4066.
33. Wiener MC, Suter RM, Nagle JF (1989) Structure of the fully hydrated gel phase of dipalmitoylphosphatidylcholine. *Biophys J* 55(2):315–325.
34. Sinha SK, Sirota EB, Garoff S, Stanley HB (1988) X-ray and neutron scattering from rough surfaces. *Phys Rev B Condens Matter* 38(4):2297–2311.
35. Swain PS, Andelman D (2001) Supported membranes on chemically structured and rough surfaces. *Phys Rev E Stat Nonlin Soft Matter Phys* 63(5 Pt 1):051911.